Desalination and Water Treatment
www.deswater.com
doi: 10.5004/dwt.2021.27134

223 (2021) 393–402
May

Removal of Congo red dye from its aqueous solutions using NiFe-LDH and GO/NiFe-LDH composite materials as adsorbent

You Wu, Zhuannian Liu*

College of Geology and Environment, Xi'an University of Science and Technology, Xi'an 710054, PR China, Tel. +86 18740417277; email: securewyy@126.com (Y. Wu), Tel. +86 13892803449; email: zhuannianliu@163.com (Z. Liu)

Received 2 December 2020; Accepted 11 February 2021

ABSTRACT

The layered double hydroxides of nickel and iron (NiFe-LDH) and graphene oxide (GO)/NiFe-LDH composite were synthesized in this paper. The adsorption properties of Congo red (CR) on the composite were compared with that of NiFe-LDH. The effects of reaction time, pH, temperature and initial concentration on the adsorption capacity of CR on these materials as well as the reusability of the material were discussed. The structure of these materials and the removal mechanism of CR on the composite material were analyzed by scanning electron microscopy, Fourier-transform infrared spectroscopy, X-ray diffraction and nitrogen adsorption-desorption analysis. The results show that the adsorption capacity of CR on the composite GO/NiFe-LDH-1% was 421.35 mg g^{-1}, which is higher than that of NiFe-LDH. The adsorption mechanism of CR is based on ion exchange, electrostatic attraction and π–π interaction. The composite adsorbent has good reusability and it is a promising adsorbent for removal of CR from aqueous environment.

Keywords: Layered double hydroxides; Adsorption; Dye; Graphene oxide; Ion exchange

1. Introduction

Due to rapid urbanization, industrialization and agricultural activities in recent decades, water pollution has gradually become a serious globally problem [1–3]. Many industries discharge their effluents into water bodies without pre-treatment which contains heavy metal ions, dyes and other organic pollutants, that threaten the human health, marine ecosystem and environment due to their toxicity, carcinogenetic, mutagenic and poisoners features [4]. Among various water pollutants, dyes have received extensive attention of researchers since till now over 100,000 synthetic types of dyes have been produced. In other word the world produces approximately 7×10^7 tons of synthetic dyes for the textile industry each year. However, 10% of the dyes are discharged into the environment as waste liquid after dyeing and processing [5,6]. Synthetic dyes are mixed with a large number of toxic and harmful substances, such as copper sulfate, lead chromate, mercury sulfide, etc. [7]. Existences of these substances over the normal range have adverse effect on environment [8–10], and humans health. Congo red is a typical organic dye, it will pollute local waters when discharged into water [11]. Therefore, water safety and converting contaminated water bodies into reusable water is one of the promising strategies for sustainable water supply [12,13]. To date, numerous strategies has been developed to treat wastewater include membrane technology [14], biological [15], photocatalytic [16], flocculation [17], adsorption [18,19], etc. Among them, adsorption has received wide attention due to its high removal efficiency, wide adsorption range, simple operation, low cost, less energy requirement and environmentally friendly [20–22].

So far, a varieties of adsorbents material with excellent performance have been researched and developed to remove pollutants from water bodies [23–27]; in particular removal of dyes by these adsorbents have been extensively studied [28–34]. Among numerous adsorbents, layered double

* Corresponding author.

hydroxides (LDHs for short, also known as hydrotalcite compounds) which are anionic clays formed by stacking layers of positively charged metal hydroxides and negatively charged anions between layers [35], proven as a promising adsorbent due to their high thermal stability, memory effect [36,37], large specific surface area and high porosity. At present, many researchers have been used this material for the treatment of dyes in wastewater [38–40], but since its monomer materials are prone to self-stacking, thus, impair the high adsorption performance of LDHs. To overcome this problem and enhance its high adsorption performance many researchers synthesized LDHs with other materials such as carbon nanotubes, montmorillonite and metal organic frameworks [41–43].

Carbon materials are one of the most widely used adsorption materials, and graphene oxide which is a carbonic material displayed excellent features in wastewater treatment [44,45] due to its large specific surface area, mechanical flexibility, thermal stability, good dispersibility, and contains a large number of oxygen-containing functional groups on its surface [46–48]. The monomer material already shown good adsorption properties [47,49]. Furthermore, graphene oxide (GO) has a strong dispersibility properties which hinder the agglomeration of composites material result in higher specific surface area and better adsorption performance of the adsorbent material [50,51].

Herein, GO is combined with NiFe-LDH, to form a coating structure with many small layers wrapped in large layers through self-assembly in the reactor, and synthesize new composite adsorbent. In this study, we prepared NiFe-LDH and GO/NiFe-LDH composites by hydrothermal method. NiFe-LDH grows on the GO surface containing a large number of oxygen-containing functional groups, which contribute in the formation of a compact coating structure. Therefore, the addition of GO hinders the phenomenon of LDH self-stacking, result in high specific surface area and increase adsorption active sites, which improves the adsorption capacity of the composite material. The optimum adsorption capacity of the composite material toward Congo red was investigated by adjusting the mass ratio of GO and NiFe-LDH to find out the best ratio of NiFe-LDH and GO/NiFe-LDH composite materials.

2. Experiment

2.1. Materials

Chemical substances used to prepare NiFe-LDH, including iron nitrate nonahydrate ($Fe(NO_3)_3{\cdot}9H_2O$), nickel nitrate hexahydrate ($Ni(NO_3)_2{\cdot}6H_2O$), urea ($CO(NH_2)_2$), and citric acid trisodium dihydrate ($Na_3C_6H_5O_7{\cdot}2H_2O$) were purchased from Sinopharm Chemical Reagent Co., Ltd., (China). Other chemicals such as, absolute ethanol, and Congo red ($C_{32}H_{22}N_6Na_2O_6S_2$) were all analytically pure and provided by Sinopharm Chemical Reagent Co., Ltd., (China). The deionized (DI) water was used for preparing the solution and washing the prepared samples.

2.2. Synthesis of NiFe-LDH and GO/NiFe-LDH

- Preparation of GO and NiFe-LDH: GO was prepared by classic Hummers method. NiFe-LDH was prepared by adding 0.909 g (2.25 mmol) $Fe(NO_3)_3{\cdot}9H_2O$, 1.9643 g (6.75 mmol) $Ni(NO_3)_2{\cdot}6H_2O$, 1.08 g (18 mmol) urea and 0.2322 g (0.9 mmol) of trisodium citrate sequentially into 70 mL of deionized water and stirred for 10 min. Then the obtained mixture was sealed and transferred to 100 mL Teflon-lined stainless-steel autoclave and placed in an oven at 150°C for 12 h, following that the dried material washed with ethanol and DI water for 6 times alternately and placed in an oven at 60°C to dry until the weight no longer decreased.
- Preparation of GO/NiFe-LDH composite adsorption material: the same procedure applied as (1), except changing the weight of 0.2%, 0.5%, 1%, 2% and 5% of the material in (1) before stirring and adding the as prepared graphene oxide to the mixture.

2.3. Characterization

The JSM-7200F (JEOL, Japan) electron microscope was used to scan the adsorbent material to observe the surface structure and microscopic composition of the adsorbent material. The XD-3 type X-ray powder diffraction was used to analysis the crystalline structure of the adsorbent material, the scanning step was 0.02°, and the scanning range 2θ was 5°~75°. A Perkin-Elmer 550 s Fourier-transform infrared spectrometer (PerkinElmer Co., Ltd., USA) was used for the infrared test, and a scanning test was performed at a wavenumber of 4,000~400 cm^{-1}. In this experiment, a JW-BK122W N_2 physical adsorption instrument (Beijing JWGB Science & Technology Co., Ltd., China) was used to test the specific surface area of the adsorbent material. The Brunauer–Emmett–Teller (BET) and Barrett–Joyner–Halenda methods were used to calculate the BET specific surface area, pore volume and pore diameter of the adsorbent materials.

2.4. Adsorption experiments

In order to adsorption capacity of the prepared adsorbent toward Congo red (CR), a solution of 100 mg L^{-1} CR was prepared and placed in a 1,000 mL volumetric flask Then, 100 mL of the prepared solution was poured in a beaker, 0.1 g of the adsorbent was added, and the samples were taken at 10, 30, 60, 90, 120, 150, and 180 min time interval after the start of adsorption. The absorbance was measured under an ultraviolet-visible spectrophotometer using UV-Vis spectroscopy at the absorption peak of 497 nm (UV-6100S double beam spectrophotometer, Shanghai Mapada Instrument and Meter Co., Ltd., China), and the concentration was then calculated. Influencing parameter such as pH, temperature, initial concentration, and dosage of the experiment were adjusted separately to explore their impact on adsorption process. The adsorption capacity and removal efficiency were calculated by the following equations:

$$q_e = \frac{\left(C_0 - C_e\right)V}{m} \tag{1}$$

$$\eta = \frac{\left(C_0 - C_t\right)}{C_0} \times 100\% \tag{2}$$

where q_e shows the adsorption equilibrium, mg g^{-1}; C_0 indicate the initial concentration of simulated wastewater, mg L^{-1}; C_e is concentration of simulated wastewater at adsorption equilibrium, mg L^{-1}; V is the volume of simulated wastewater, L; m is the mass of the adsorbent; η is adsorption efficiency, %; C_0 is initial mass concentration of CR solution, mg L^{-1}; and C_t is the mass concentration of CR after adsorption, mg L^{-1}.

3. Results and discussion

3.1. Morphology and microstructure

The scanning electron microscopy (SEM) images of GO/NiFe-LDH-1% are shown in Figs. 1a and b. The small pieces of NiFe-LDH are assembled and synthesized on the surface of GO, and the GO is completely covered. The morphology of NiFe-LDH and GO is similar to the previous research results [52–54], which proves that we successfully synthesized these two materials and assembled them together. The addition of GO makes the arrangement of NiFe-LDH more uniform and orderly, reduces the self-stacking phenomenon that occurs in NiFe-LDH itself [55], which result in presence of more active groups on the surface material and enhanced adsorption performance. The SEM images of GO/NiFe-LDH-5% is shown in Figs. 1c and d. Compared with GO/NiFe-LDH-1%, the LDH lamella in this figure is significantly reduced, and there is a considerable part of the lamella that is not completely formed, it is due the larger GO sheet which will block the combination and reaction of LDH precursor materials and affect the quality of the composite material. This proves that excessive GO will inhibit the synthesis of NiFe-LDH, it's also reflected in the adsorption kinetics analysis. Certainly, adding a small amount of GO to NiFe-LDH may have positive effect since it arranged the LDH slices over the GO and prevent the reduction of active groups caused by self-stacking. While excessive GO will block the synthesis of NiFe-LDH precursor materials, making it difficult to form smoothly. Therefore, it is necessary to discuss the optimal ratio.

3.2. Crystal structure

The crystal structure of the adsorbent is shown in Fig. 2. The diffraction peaks of the NiFe-LDH sample were located at 11.3°, 23.0°, 34.0°, 39.3°, 46.1°, 61.0° and 65.4°. These diffraction peaks can be attributed to (003), (006), (012), (015), (110), (113), (116), which indicate that the

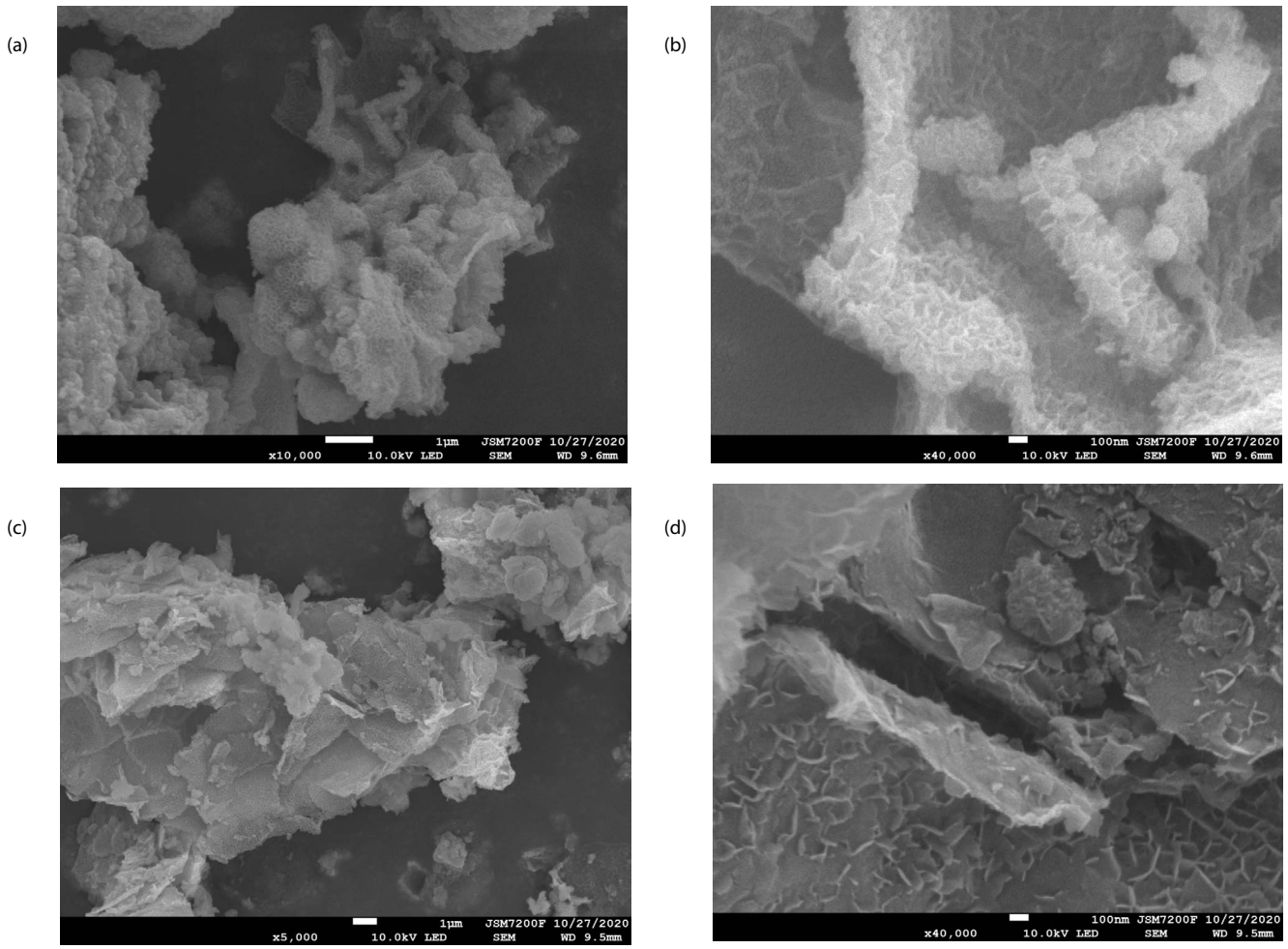

Fig. 1. SEM images of the GO-NiFe-LDH-1% (a and b); GO-NiFe-LDH-5% (c and d).

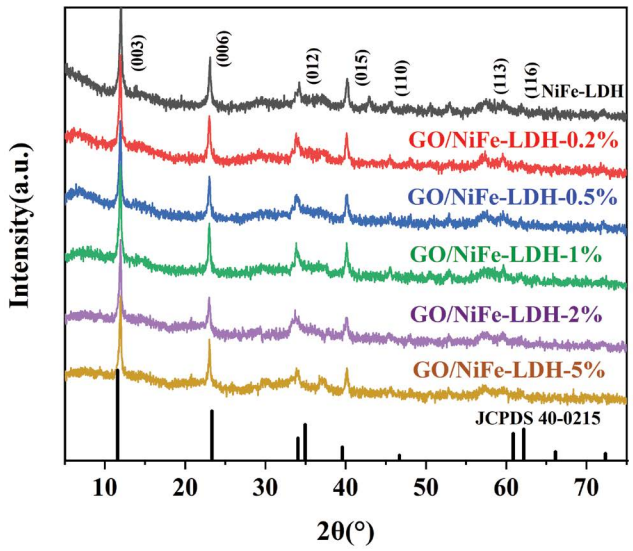

Fig. 2. X-ray diffraction patterns of samples.

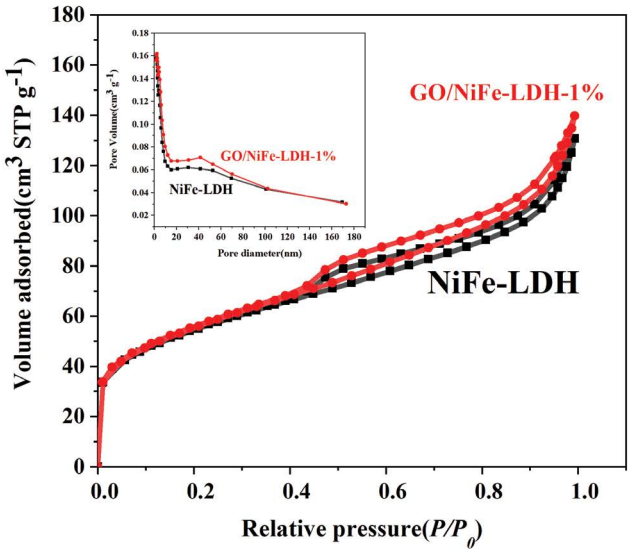

Fig. 3. N_2 adsorption–desorption isotherms and corresponding pore size distribution curves (inset) of samples.

samples we prepared were nickel-iron hydrotalcite with a diamond structure (JCPDS No.40-0215) [56]. Compared with the standard card, the diffraction peak was slightly shifted, which was caused by different anions embedded in the interlayer. The remaining curves show diffraction peaks similar to NiFe-LDH, indicating the presence of NiFe-LDH in the composite material. It can be seen that GO/NiFe-LDH doped with different proportions of GO, while it still retains the crystalline structure.

3.3. Nitrogen adsorption–desorption analysis

It can be seen from Fig. 3 that the two isotherms rose sharply when the pressure was close to P_0, and dropped steeply in the middle pressure section during desorption. In addition, similar hysteresis loops were detected in both samples. Based on Fig. 3, it is a typical type IV adsorption–desorption isotherm. The characteristic of the line proves that it has a typical mesoporous structure, and the adsorption hysteresis ring is H4 type, which indicating that the adsorbent contains narrow slit pores and uniform pore size distribution. The addition of GO makes the NiFe-LDH arrangement more orderly and hinder the specific surface area reduction caused by agglomeration. Therefore, the specific surface area increases from 194.82 to 198.14 $m^2\ g^{-1}$. The pore volumes of NiFe-LDH and GO/NiFe-LDH are 0.20 and 0.22 $cm^3\ g^{-1}$, respectively, and the pore diameters are 5.47 and 5.36 nm, respectively. This indicates that the two composite have similar pore structure and porosity, which is aligned with the previous studies [42].

3.4. Fourier-transform infrared spectroscopy analysis

As shown in Fig. 4, the Fourier-transform infrared spectroscopy (FTIR) of GO contained two characteristic peaks near 1,611 and 1,719 cm^{-1} respectively. These two characteristic peaks are associated to the oxygen functional groups on the GO surface (such as C=O and –OH). The FTIR of NiFe-LDH showed different FTIR patterns,

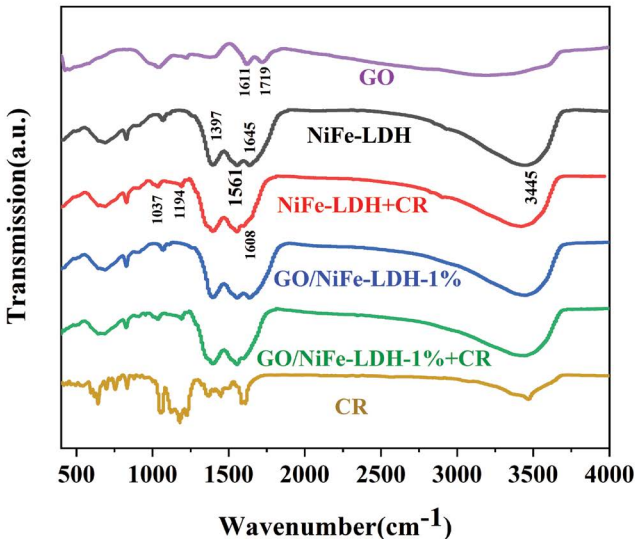

Fig. 4. FTIR spectra of samples.

with characteristic peaks at 1,070; 1,397; 1,561; 1,645 and 3,445 cm^{-1} respectively. The broad peak at 3,445 cm^{-1}, and the peaks at 1,645 and 1,561 cm^{-1} are correspond to the hydroxyl (–OH) in the water adsorbed on the sample surface. The strong peak at 1,397 cm^{-1} was symmetrical to CO_3^{2-}. The stretching mode was related, mainly from the decomposition and conversion of urea. The absorption peak below 1,000 cm^{-1} could be attributed to the lattice vibration of M–O–M and M–O (M standing for Fe or Ni). GO/NiFe-LDH retained the crystal structure of NiFe-LDH, and characteristic peaks of the two. After the two samples adsorbed the CR, several new absorption peaks appeared near 1,037; 1,196 and 1,608 cm^{-1}. The peak at 1,608 cm^{-1} originated from the tensile vibration of the C=C bond in the CR molecule. The other two peaks came from the S=O tensile shock in the CR sulfonic acid group which proved that CR

was successfully adsorbed to the surface of GO/NiFe-LDH and NiFe-LDH.

3.5. Effect of pH

It can be seen from Fig. 5 that under different pH conditions, the adsorption capacity of GO/NiFe-LDH-1% on CR is much higher than that of NiFe-LDH. As the pH value increased, the adsorption capacity of both on CR gradually decreased. When the pH value was less than 7, the solution contained a large amount of H^+, and the H^+ combined with the surface functional groups of NiFe-LDH to form a positively charged.

3.6. Adsorption kinetics

It can be seen from Fig. 6 that the adsorption rate was very fast before 30 min. This is due to presence of a large number of active sites on the surface of samples, which could quickly adsorb CR. With the increasing of time, most of the adsorption active sites were gradually occupied, and the adsorption rate slowed down until it finally reaches equilibrium about 180 min. When GO < 1%, the addition of GO does not significantly improve the adsorption performance of NiFe-LDH. When it is >1%, the synthesis of NiFe-LDH is greatly inhibited, so 1% is the ratio that enables it to play the best performance. The Lagergren pseudo-first-order reaction kinetic model and the pseudo-second-order reaction kinetic model were used to compare samples. The experimental data of adsorption CR was fitted for both. The linear form of the Lagergren pseudo-first-order adsorption kinetic equation is calculate as below:

$$\log\left(q_e - q_t\right) = \log q_e - \frac{k_1}{2.303}t \tag{3}$$

where q_t is the adsorption capacity at time t, mg g^{-1}; q_e is the equilibrium adsorption capacity, mg g^{-1}; k_1 is the pseudo-first-order adsorption rate constant, min^{-1}.

The pseudo-second-order reaction rate equation:

$$\frac{t}{q_t} = \frac{1}{k_2 q_e^2} + \frac{1}{q_e}t \tag{4}$$

The Lagergren pseudo-first-order and pseudo-second-order reaction rate equations were used to process the data in Fig. 6 and the results are shown in Fig. 7. The regression parameters are shown in Table 1. It can be seen from Table 1 that the degree of fitting between the adsorption of CR and the Lagergren pseudo-second-order adsorption kinetic model was higher, and the linear correlation coefficient R^2 were 0.99956 and 0.99727, respectively.

3.7. Adsorption isotherms

Fig. 8 shows the adsorption isotherms of samples. It can be seen from the figure that when C_e was low, the adsorption site filling rate of the adsorbent to CR was low. With the increase in concentration, the filling rate gradually increased, the adsorption gradually reached saturation, and the adsorption effect of GO/NiFe-LDH-1% was better than NiFe-LDH on CR.

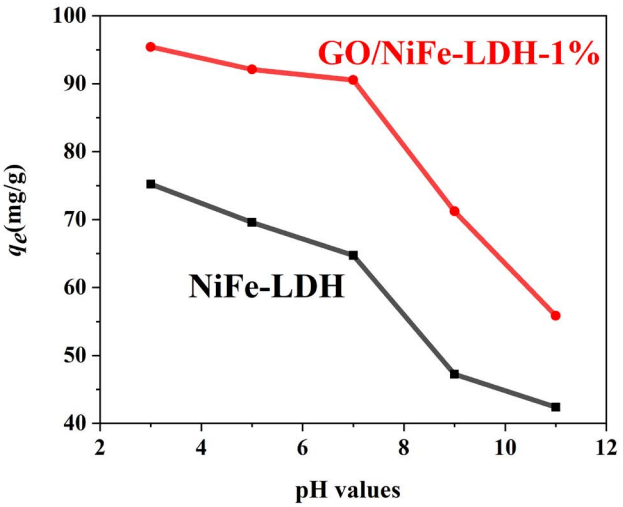

Fig. 5. Effect of pH on adsorption of CR onto samples.

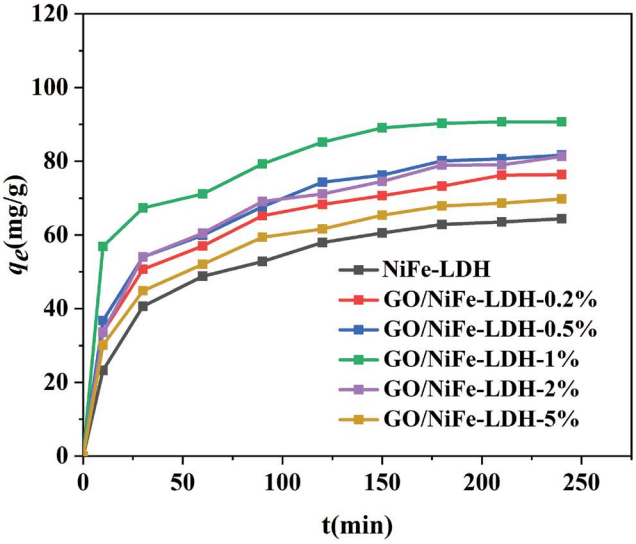

Fig. 6. Adsorption of CR onto samples at different adsorption times.

The Langmuir isotherm model and the Freundlich isotherm model were used to process the data in Fig. 8, and the results are shown in Fig. 9. The regression parameters are shown in Table 2.

It can be seen that the adsorption of CR by the two samples has a high degree of fit with the Langmuir isotherm model, and the linear correlation coefficient R^2 was greater than the Freundlich isotherm model; which indicated that the adsorption monolayer.

The Langmuir isotherm equation is:

$$\frac{1}{q_e} = \frac{1}{Q_0} + \left(\frac{1}{bQ_0}\right)\left(\frac{1}{C_e}\right) \tag{5}$$

Table 1
Parameters in the two kinetic models for CR adsorption by NiFe-LDH and GO/NiFe-LDH-1% composite

Adsorbents	q_e (mg g^{-1})	Pseudo-first-order model			Pseudo-second-order model		
		k_1 (min^{-1})	$q_{e,c}$ (mg g^{-1})	R^2	k_2 (g mg^{-1} min^{-1})	$q_{e,c}$ (mg g^{-1})	R^2
NiFe-LDH	64.4	0.0180	46.73	0.9847	0.00058	70.62	0.9996
GO/NiFe-LDH-1%	90.71	0.0310	96.37	0.8952	0.00078	96.06	0.9973

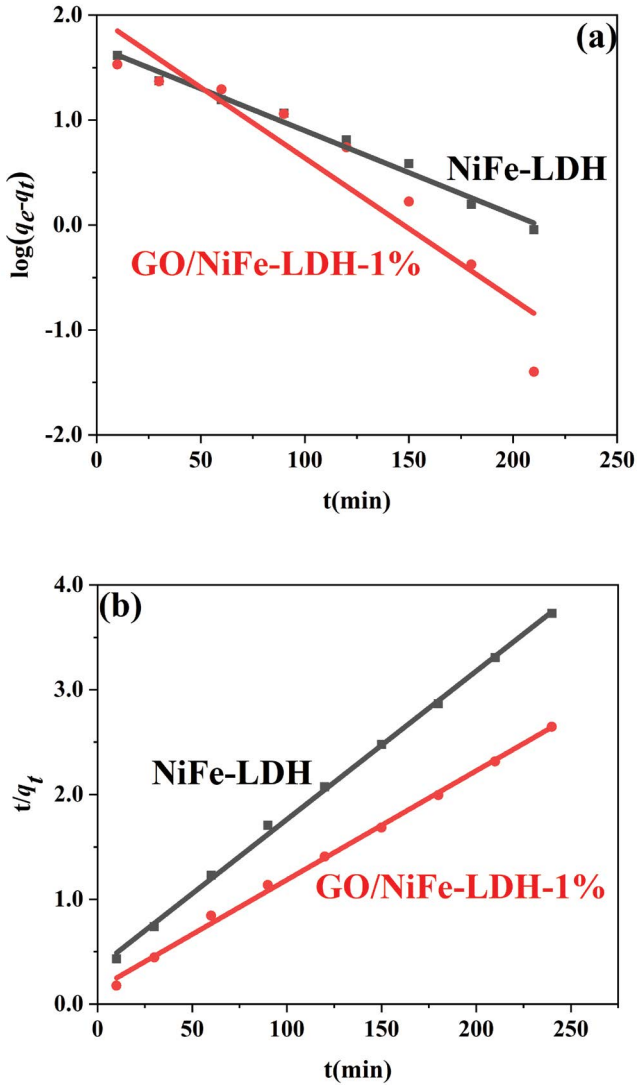

Fig. 7. Lagergren first-order (a) and second-order (b) kinetics equation plot.

where Q_0 is the unit saturated adsorption capacity when forming the monolayer adsorption, mg g^{-1}; C_e is the equilibrium mass concentration of the solution, mg L^{-1}; q_e is the equilibrium adsorption capacity, mg g^{-1}; b is the Langmuir equilibrium constant.

The Freundlich isotherm equation is:

$$\log q_e = \log K_F + \frac{1}{n}\log C_e \quad (6)$$

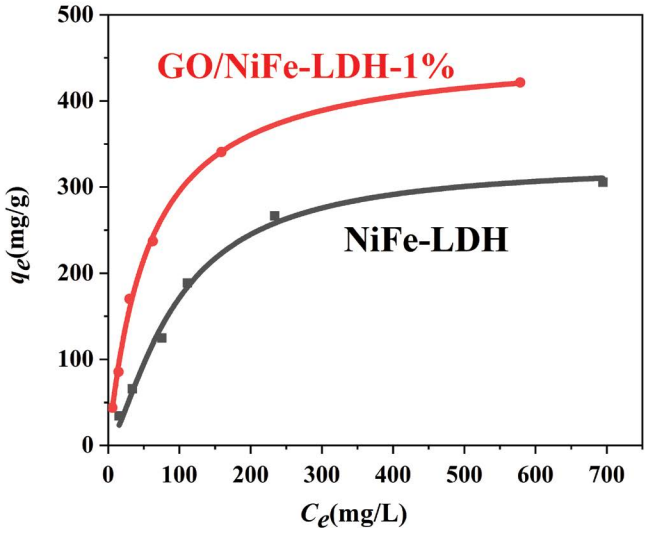

Fig. 8. CR adsorption isotherms for samples.

where K_F and n are adsorption constants related to factors such as temperature and specific surface area of the adsorbent.

3.8. Adsorption thermodynamics

It can be seen from Fig. 10 that with an increase in temperature, the adsorption capacity of the adsorbent on CR gradually decreases. Hence the higher temperature is not conducive to the progress of the reaction. When the temperature is high, it may cause changes in the adsorbent and affect the adsorption capacity.

The fitting data of the thermodynamic model is shown in Fig. 11, and according to the following adsorption thermodynamic formula, we can get the relevant thermodynamic parameters of NiFe-LDH as well as GO/NiFe-LDH-1% adsorbents adsorbing CR.

$$\Delta G = \Delta H - T\Delta S \quad (7)$$

where ΔG is the Gibbs free energy change, J mol^{-1}; ΔH is the adsorption enthalpy change, J mol^{-1}; ΔS is the adsorption entropy change, J K^{-1} mol^{-1}; T is the thermodynamic temperature, meanwhile K is the unit of the temperature and calculated according to the following equation.

$$\log K_d = \frac{\Delta S}{R} - \frac{\Delta H}{2.303RT} \quad (8)$$

Table 2
Parameters of the Langmuir and Freundlich isotherm models for CR adsorption onto the samples

Adsorbents	Langmuir			Freundlich		
	Q_0 (mg g^{-1})	b (L mg^{-1})	R^2	K_F	n	R^2
NiFe-LDH	370.37	0.0064	0.9974	8.22	1.66	0.9186
GO/NiFe-LDH-1%	471.70	0.0163	0.9975	23.44	1.99	0.9119

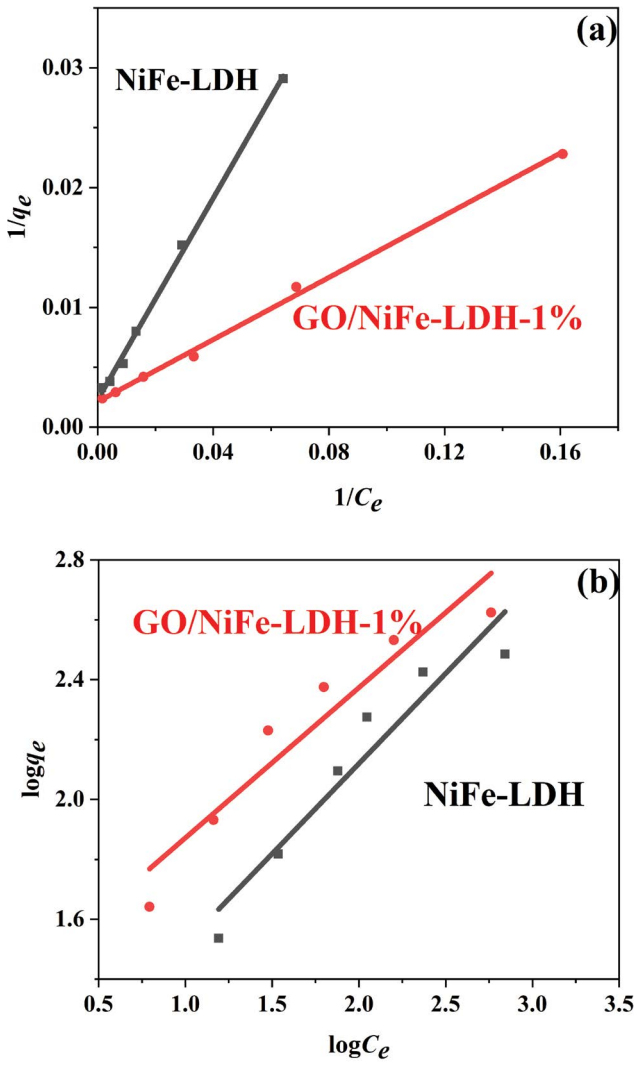

Fig. 9. Fitting results of linearized Langmuir (a) and Freundlich (b) adsorption isotherms of CR adsorption on samples.

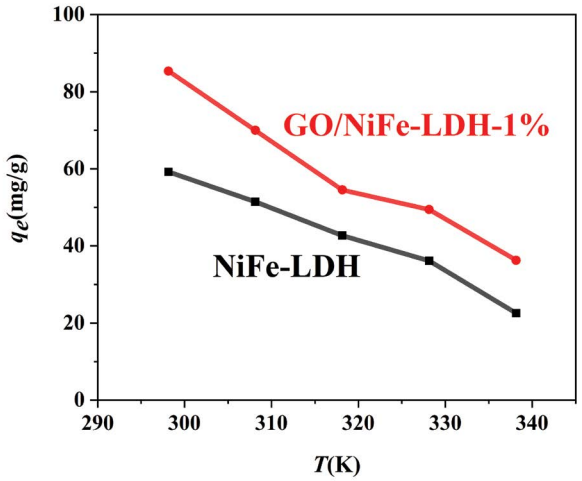

Fig. 10. Effects of different temperatures on CR adsorption.

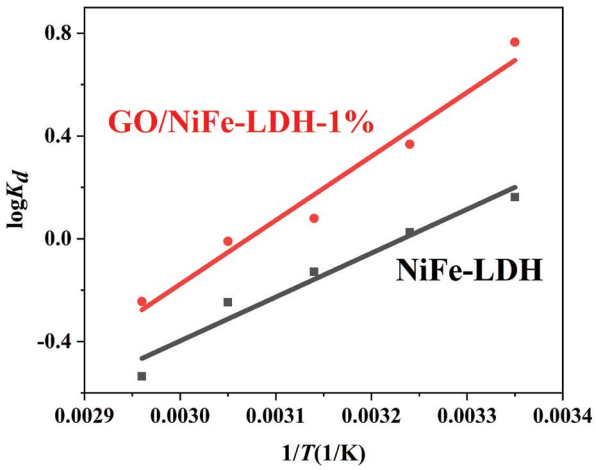

Fig. 11. The logK_d~1/T relation diagram of CR adsorbed by adsorbent.

where K_d is the distribution coefficient and R is the thermodynamic constant, taking 8.314 J K^{-1} mol^{-1}.

The fitting results are shown in Fig. 11, and the parameters are shown in Table 3. It can be seen from Table 3 that the ΔH during the adsorption of CR by NiFe-LDH and GO/NiFe-LDH-1% were negative; which indicate that the reaction of samples when adsorbing CR was an exothermic response. This was consistent with the results shown in Fig. 10.

ΔS was a negative value, which indicates that the disorder at the solid–liquid interface decreased when CR was adsorbed by NiFe-LDH and GO/NiFe-LDH-1%. When ΔG was negative, it was a spontaneous process. In summary, NiFe-LDH and GO/NiFe-LDH-1% adsorption of CR were spontaneous thermal reactions.

3.9. Adsorption mechanism

Acidic conditions promote the adsorption process, so there is electrostatic attraction between the negatively charged CR and GO/NiFe-LDH-1% surface. LDH has interlayer anion exchange, thus CR can also exchange anions

Table 3
Thermodynamic parameters of CR adsorption on NiFe-LDH and GO/NiFe-LDH-1%

Adsorbents	T (K)	ΔG (kJ mol^{-1})	ΔH (kJ mol^{-1})	ΔS (J (K mol)$^{-1}$)
NiFe-LDH	298.15	–19.02	–32.71	–45.92
	308.15	–18.56		
	318.15	–18.10		
	328.15	–17.64		
	338.15	–17.18		
GO/NiFe-LDH-1%	298.15	–28.72	–47.67	–63.57
	308.15	–28.08		
	318.15	–27.45		
	328.15	–26.81		
	338.15	–26.17		

between LDH layers to achieve the purpose of adsorption. CR molecule contains a benzene ring, which can promote adsorption through π–π interaction with GO. In short, the main adsorption mechanism of GO/NiFe-LDH-1% to CR is electrostatic attraction, ion exchange and π–π interaction.

3.10. Recycle adsorption experiments

The results of recycle adsorption experiments are shown in Fig. 12. It can be seen that after 4 times of reuse, the adsorption capacity of NiFe-LDH and GO/NiFe-LDH-1% adsorbents on CR continued to decrease, and the removal rate of CR by NiFe-LDH dropped from 80.26% to 34.84%. The removal rate of CR by NiFe-LDH-1% decreased from 94.1% to 40.16%, indicating that the adsorbent has a good reproducibility and reusability.

4. Conclusions

In this work, GO/NiFe-LDH composite adsorbent was successfully synthesized through hydrothermal reaction. GO/NiFe-LDH has a "sandwich biscuit" structure. The existence of GO improves the self-stacking phenomenon of NiFe-LDH, and provide more active sites, result in high adsorption capacity. GO/NiFe-LDH-1% ratio displayed the highest removal rate (90.71%) toward CR. The adsorption kinetic experiment showed that the adsorption process is a single-layer adsorption. The adsorption isotherm experiment displayed that the adsorption process is more similar to the Langmuir model. Moreover, the adsorption thermodynamic experiment indicated that the adsorption process emits heat spontaneously. The adsorption effect of GO/NiFe-LDH-1% is far better than that of NiFe-LDH, and the composite material exhibited certain potential for treatment of wastewater.

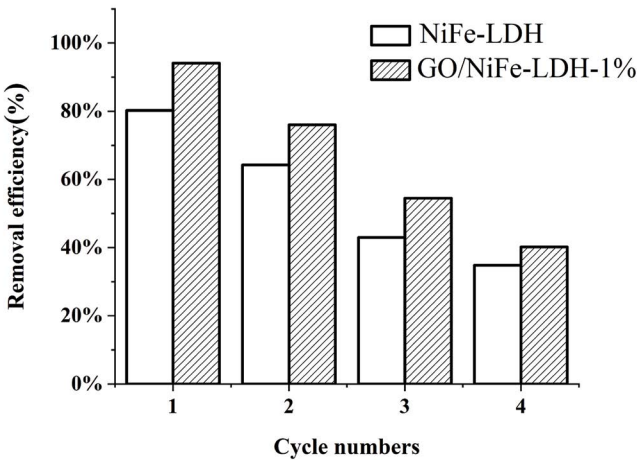

Fig. 12. Regeneration cycles of samples.

Acknowledgement

The research was supported by the National Natural Science Foundation of China (51278418).

References

[1] C.S. Santana, D.M. Montalván Olivares, V.H.C. Silva, F.H.M. Luzardo, F.G. Velasco, R.M. de Jesus, Assessment of water resources pollution associated with mining activity in a semi-arid region, J. Environ. Manage., 273 (2020) 111148, doi: 10.1016/j.jenvman.2020.111148.
[2] M. Strokal, C. Kroeze, Water, society and pollution in an urbanizing world: recent developments and future challenges, Curr. Opin. Environ. Sustainability, 46 (2020) 11–15.
[3] A. Deletic, H.T. Wang, Water pollution control for sustainable development, Chem. Eng., 5 (2019) 839–840.
[4] T.O. Ajiboye, O.A. Oyewo, D.C. Onwudiwe, Simultaneous removal of organics and heavy metals from industrial wastewater: a review, Chemosphere, 262 (2021) 128379, doi: 10.1016/j.chemosphere.2020.128379.
[5] V. Katheresan, J. Kansedo, S.Y. Lau, Efficiency of various recent wastewater dye removal methods: a review, J. Environ. Chem. Eng., 6 (2018) 4676–4697.
[6] B.-M. Jun, J.Y. Heo, N. Taheri-Qazvini, C.M. Park, Y.M. Yoon, Adsorption of selected dyes on $Ti_3C_2T_x$ MXene and Al-based metal-organic framework, Ceram. Int., 46 (2020) 2960–2968.
[7] J. Mittal, Permissible synthetic food dyes in India, Resonance, 25 (2020) 567–577.
[8] V.K. Gupta, Suhas, Application of low-cost adsorbents for dye removal – a review, J. Environ. Manage., 90 (2009) 2313–2342.
[9] M.A. Rauf, S.S. Ashraf, Survey of recent trends in biochemically assisted degradation of dyes, Chem. Eng. J., 209 (2012) 520–530.
[10] L. Tang, J.F. Yu, Y. Pang, G.M. Zeng, Y.C. Deng, J.J. Wang, X.Y. Ren, S.J. Ye, B. Peng, H.P. Feng, Sustainable efficient adsorbent: alkali-acid modified magnetic biochar derived from sewage sludge for aqueous organic contaminant removal, Chem. Eng. J., 336 (2018) 160–169.
[11] C. Thamaraiselvan, M. Noel, Membrane processes for dye wastewater treatment: recent progress in fouling control, Crit. Rev. Env. Sci. Technol., 45 (2015) 1007–1040.
[12] M. Rafatullah, O. Sulaiman, R. Hashim, A. Ahmad, Adsorption of methylene blue on low-cost adsorbents: a review, J. Hazard. Mater., 177 (2010) 70–80.
[13] C. Tortajada, P. van Rensburg, Drink more recycled wastewater, Nature, 577 (2020) 26.
[14] M. Hernández-Zamora, H.V. Perales-Vela, C.M. Flores-Ortíz, R.O. Cañizares-Villanueva, Physiological and biochemical responses of *Chlorella vulgaris* to Congo red, Ecotoxicol. Environ. Saf., 108 (2014) 72–77.
[15] M.A.M. Al-Alwani, N.A. Ludin, A.B. Mohamad, A.A.H. Kadhum, A. Mukhlus, Application of dyes extracted from *Alternanthera dentata* leaves and *Musa acuminata* bracts as natural sensitizers for dye-sensitized solar cells, Spectrochim. Acta, Part A, 192 (2018) 487–498.

[16] E. Forgacs, T. Cserháti, G. Oros, Removal of synthetic dyes from wastewaters: a review, Environ. Int., 30 (2004) 953–971.
[17] C.R. Holkar, A.J. Jadhav, D.V. Pinjari, N.M. Mahamuni, A.B. Pandit, A critical review on textile wastewater treatments: possible approaches, J. Environ. Manage., 182 (2016) 351–366.
[18] M.T. Yagub, T.K. Sen, S. Afroze, H.M. Ang, Dye and its removal from aqueous solution by adsorption: a review, Adv. Colloid Interface Sci., 209 (2014) 172–184.
[19] A. Hethnawi, N.N. Nassar, A.D. Manasrah, G. Vitale, Polyethylenimine-functionalized pyroxene nanoparticles embedded on diatomite for adsorptive removal of dye from textile wastewater in a fixed-bed column, Chem. Eng. J., 320 (2017) 389–404.
[20] K.A. Adegoke, O.S. Bello, Dye sequestration using agricultural wastes as adsorbents, Water Resour. Ind., 12 (2015) 8–24.
[21] G. Crini, Non-conventional low-cost adsorbents for dye removal: a review, Bioresour. Technol., 97 (2006) 1061–1085.
[22] A. Srinivasan, T. Viraraghavan, Decolorization of dye wastewaters by biosorbents: a review, J. Environ. Manage., 91 (2010) 1915–1929.
[23] A. Mittal, R. Ahmad, I. Hasan, Poly(methyl methacrylate)-grafted alginate/Fe_3O_4 nanocomposite: synthesis and its application for the removal of heavy metal ions, Desal. Water Treat., 57 (2016) 19820–19833.
[24] A. Mittal, R. Ahmad, I. Hasan, Biosorption of Pb^{2+}, Ni^{2+} and Cu^{2+} ions from aqueous solutions by L-cystein-modified montmorillonite-immobilized alginate nanocomposite, Desal. Water Treat., 57 (2016) 17790–17807.
[25] H. Daraei, A. Mittal, M. Noorisepehr, F. Daraei, Kinetic and equilibrium studies of adsorptive removal of phenol onto eggshell waste, Environ. Sci. Pollut. Res., 20 (2013) 4603–4611.
[26] Z.N. Liu, A.P. Fan, C.-H. Ho, Preparation of AC/Cu-BTC composite and its adsorption mechanisms, J. Environ. Eng., 146 (2020) 04020018.
[27] Z.N. Liu, A.P. Fan, X.G. Han, H. Shapour, Q.Y. Zhang, PEI-modified chromium-based metal organic framework for Cr(VI) removal from aqueous solution, Desal. Water Treat., 184 (2020) 139–149.
[28] I. Anastopoulos, A. Mittal, M. Usman, J. Mittal, G.H. Yu, A. Núñez-Delgado, M. Kornaros, A review on halloysite-based adsorbents to remove pollutants in water and wastewater, J. Mol. Liq., 269 (2018) 855–868.
[29] C. Arora, S. Soni, S. Sahu, J. Mittal, P. Kumar, P.K. Bajpai, Iron based metal organic framework for efficient removal of methylene blue dye from industrial waste, J. Mol. Liq., 284 (2019) 343–352.
[30] S. Soni, P.K. Bajpai, J. Mittal, C. Arora, Utilisation of cobalt doped iron based MOF for enhanced removal and recovery of methylene blue dye from waste water, J. Mol. Liq., 314 (2020) 113642.
[31] V.K. Gupta, S. Agarwal, R. Ahmad, A. Mirza, J. Mittal, Sequestration of toxic Congo red dye from aqueous solution using ecofriendly guar gum/activated carbon nanocomposite, Int. J. Biol. Macromol., 158 (2020) 1310–1318.
[32] J. Mittal, V. Thakur, A. Mittal, Batch removal of hazardous azo dye Bismark Brown R using waste material hen feather, Ecol. Eng., 60 (2013) 249–253.
[33] V. Kumar, P. Saharan, A.K. Sharma, A. Umar, I. Kaushal, A. Mittal, Y. Al-Hadeethi, B. Rashad, Silver doped manganese oxide-carbon nanotube nanocomposite for enhanced dye-sequestration: isotherm studies and RSM modelling approach, Ceram. Int., 46 (2020) 10309–10319.
[34] A. Mittal, V. Thakur, V. Gajbe, Evaluation of adsorption characteristics of an anionic azo dye Brilliant Yellow onto hen feathers in aqueous solutions, Environ. Sci. Pollut. Res., 19 (2012) 2438–2447.
[35] S. Mallakpour, M. Hatami, C.M. Hussain, Recent innovations in functionalized layered double hydroxides: fabrication, characterization, and industrial applications, Adv. Colloid Interface Sci., 283 (2020) 102216.
[36] R. Zhang, Y.J. Ai, Z.H. Lu, Application of multifunctional layered double hydroxides for removing environmental pollutants: recent experimental and theoretical progress, J. Environ. Chem. Eng., 8 (2020) 103908.
[37] A. Chatterjee, P. Bharadiya, D. Hansora, Layered double hydroxide based bionanocomposites, Appl. Clay Sci., 177 (2019) 19–36.
[38] J.H. Cui, C.L. Wei, M. Zhang, J. Zhu, F.X. Li, X.H. Du, L.M. Chen, C.G. Li, 2D to 3D controllable synthesis of three Zn-Co-LDHs for rapid adsorption of MO by TEA-assisted hydrothermal method, Appl. Surf. Sci., 534 (2020) 147564.
[39] L. EL Mersly, El.M. El Mouchtari, El.M. Moujahid, C. Forano, M.El. Haddad, S. Briche, A.A. Tahiri, S. Rafqah, ZnCr-LDHs with dual adsorption and photocatalysis capability for the removal of acid orange 7 dye in aqueous solution, J. Sci. – Adv. Mater. Dev., 6 (2021) 118–126.
[40] Q.L. Sun, M. Tang, P.V. Hendriksen, B. Chen, Biotemplated fabrication of a 3D hierarchical structure of magnetic $ZnFe_2O_4$/MgAl-LDH for efficient elimination of dye from water, J. Alloys Compd., 829 (2020) 154552.
[41] M.T. Amin, A.A. Alazba, M. Shafiq, LDH of NiZnFe and its composites with carbon nanotubes and data-palm biochar with efficient adsorption capacity for RB5 dye from aqueous solutions: isotherm, kinetic, and thermodynamics studies, Curr. Appl. Phys., (2020) (in Press).
[42] D.B. Jiang, C. Jing, Y.S. Yuan, L. Feng, X.Y. Liu, F. Dong, B.Q. Dong, Y.X. Zhang, 2D-2D growth of NiFe LDH nanoflakes on montmorillonite for cationic and anionic dye adsorption performance, J. Colloid Interface Sci., 540 (2019) 398–409.
[43] S. Saghir, Z.G. Xiao, Hierarchical mesoporous ZIF-67@LDH for efficient adsorption of aqueous Methyl Orange and Alizarine Red S, Powder Technol., 377 (2021) 453–463.
[44] V.A. Nebol'sin, V. Galstyan, Y.E. Silina, Graphene oxide and its chemical nature: multi-stage interactions between the oxygen and graphene, Surf. Interfaces, 21 (2020) 100763, doi: 10.1016/j.surfin.2020.100763.
[45] Y.H. Tian, Z.C. Yu, L.Y. Cao, X.L. Zhang, C.H. Sun, D.W. Wang, Graphene oxide: an emerging electromaterial for energy storage and conversion, J. Energy Chem., 55 (2021) 323–344.
[46] Al.E. Burakov, E.V. Galunin, I.V. Burakova, A.E. Kucherova, S. Agarwal, A.G. Tkachev, V.K. Gupta, Adsorption of heavy metals on conventional and nanostructured materials for wastewater treatment purposes: a review, Ecotoxicol. Environ. Saf., 148 (2018) 702–712.
[47] K.C. Lai, L.Y. Lee, B.Y. Zhang, Hiew, S.T. Gopakumar, S.Y. Gan, Environmental application of three-dimensional graphene materials as adsorbents for dyes and heavy metals: review on ice-templating method and adsorption mechanisms, J. Environ. Sci., 79 (2019) 174–199.
[48] Y.T. Li, W.M. Ju, L. Yang, L.L. Zhang, Y.J. Sun, Adsorption behaviors and mechanism of graphene oxide for silver complex anion removal, Appl. Surf. Sci., 529 (2020) 147112.
[49] Y.A.R. Lebron, V.R. Moreira, G.P. Drumond, G.C.F. Gomes, M.M. da Silva, R. de Oliveira Bernardes, R.S. Jacob, M.M. Viana, C.K.B. de Vasconcelos, L.V. de Souza Santos, Statistical physics modeling and optimization of norfloxacin adsorption onto graphene oxide, Colloid. Surf., A, 606 (2020) 125534.
[50] Y. Zhang, H.J. Li, M.C. Li, M.H. Xin, Adsorption of aniline on aminated chitosan/graphene oxide composite material, J. Mol. Struct., 1209 (2020) 127973.
[51] B.L. Guo, Y. Kamura, P. Koilraj, K. Sasaki, Co-sorption of Sr^{2+} and SeO_4^{2-} as the surrogate of radionuclide by alginate-encapsulated graphene oxide-layered double hydroxide beads, Environ. Res., 187 (2020) 109712.
[52] F. Khodam, Z. Rezvani, A.R.A. Ghadim, Enhanced adsorption of Acid Red 14 by co-assembled LDH/MWCNTs nanohybrid: optimization, kinetic and isotherm, J. Ind. Eng. Chem., 21 (2015) 1286–1294.
[53] H. Chen, T.L. Liu, Y. Meng, Y. Cheng, J. Lu, H.S. Wang, Novel graphene oxide/aminated lignin aerogels for enhanced adsorption of malachite green in wastewater, Colloid. Surf., A, 603 (2020) 125281.
[54] H.J. Hu, S. Wageh, A.A. Al-Ghamdi, S.B. Yang, Z.F. Tian, B. Cheng, W.K. Ho, NiFe-LDH nanosheet/carbon fiber

nanocomposite with enhanced anionic dye adsorption performance, Appl. Surf. Sci., 511 (2020) 145570.
[55] Y.Q. Zheng, B. Cheng, W. You, J.G. Yu, W.K. Ho, 3D hierarchical graphene oxide-NiFe LDH composite with enhanced adsorption affinity to Congo red, methyl orange and Cr(VI) ions, J. Hazard. Mater., 369 (2019) 214–225.
[56] X.Y. Wang, Y.X. Tuo, Y. Zhou, D. Wang, S.T. Wang, J. Zhang, Ta-doping triggered electronic structural engineering and strain effect in NiFe LDH for enhanced water oxidation, Chem. Eng. J., 403 (2021) 126297.